Mean temperature profiles in turbulent internal flows

Pirozzoli, Sergio; Modesti, Davide

DOI
10.1016/j.ijheatfluidflow.2024.109544

Publication date
2024

Document Version
Final published version

Published in
International Journal of Heat and Fluid Flow

International Journal of Heat and Fluid Flow 109 (2024) 109544

Contents lists available at ScienceDirect

International Journal of Heat and Fluid Flow

journal homepage: www.elsevier.com/locate/ijhff

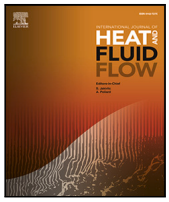

Mean temperature profiles in turbulent internal flows

Sergio Pirozzoli [a], Davide Modesti [b,*]

[a] Dipartimento di Ingegneria Meccanica e Aerospaziale, Sapienza Universitá di Roma, via Eudossiana 18, 00184 Roma, Italy
[b] Faculty of Aerospace Engineering, Delft University of Technology, Kluyverweg 2, 2629 HS Delft, The Netherlands

ARTICLE INFO

Dataset link: http://newton.dma.uniroma1.it/, http://www.thermoturb.com

Keywords:
Heat transfer
Forced convection
Internal flows
Direct numerical simulation

ABSTRACT

We derive explicit formulas for the mean profiles of temperature (modeled as a passive scalar) in forced turbulent convection, as a function of the Reynolds and Prandtl numbers. The derivation leverages on the observed universality of the inner-layer thermal eddy diffusivity with respect to Reynolds and Prandtl number variations and across different flows, and on universality of the passive scalar defect in the core flow. Matching of the inner- and outer-layer expression yields a smooth compound mean temperature profile. We find excellent agreement of the analytical profile with data from direct numerical simulations of pipe and channel flows under various thermal forcing conditions, and over a wide range of Reynolds and Prandtl numbers.

1. Introduction

The exploration of passive scalars within turbulent flows bounded by walls holds significant practical implications. It plays a crucial role in comprehending the behavior of diluted contaminants and serves as a model for temperature distribution assuming low Mach numbers and minimal temperature disparities (Monin and Yaglom, 1971; Cebeci and Bradshaw, 1984). Nonetheless, quantifying minute temperature differences and the concentration of passive tracers poses formidable challenges, leading to restricted insights into fundamental passive scalar statistics (Gowen and Smith, 1967; Kader, 1981; Subramanian and Antonia, 1981; Nagano and Tagawa, 1988).

The investigation of passive scalars in turbulent flows predominantly centers on scenarios where the Prandtl number (Pr) approaches unity, representing the ratio of kinematic viscosity to thermal diffusivity ($\mathrm{Pr} = \nu/\alpha$). Numerous studies have discussed the close similarities between the passive scalar field and the streamwise velocity field under these conditions (Kim et al., 1987; Abe and Antonia, 2009; Antonia et al., 2009). However, various fluids, including water, engine oils, glycerol, and polymer melts, exhibit Prandtl numbers significantly exceeding unity, while liquid metals and molten salts have markedly lower Prandtl numbers.

For the diffusion of contaminants, the role of the Prandtl number is replaced by the Schmidt number, which denotes the ratio of kinematic viscosity to mass diffusivity. In practical applications, the Schmidt number typically far exceeds unity (Levich, 1962). In such instances, the resemblance between velocity and passive scalar fluctuations is significantly compromised, rendering predictions of even fundamental flow properties notably challenging.

Regarding wall fluxes, the most robust framework established to date is attributed to the work by Kader and Yaglom (1972). Drawing upon universality arguments, these authors derived a predictive law for the nondimensional flux (Nusselt number) as a function of the Prandtl number. This framework primarily involves modeling the logarithmic offset function, which represents the Prandtl-dependent additive constant in the overlap-layer mean passive scalar profiles. Despite the solidity of this framework, semi-empirical power-law correlations (Dittus and Boelter, 1933; Kays et al., 1980) continue to find widespread usage in engineering design. As for the mean profiles of passive scalars, the most comprehensive study available can be traced back to the work of Kader (1981). In this study, an empirical interpolation formula was derived, connecting the universal near-wall conductive layer with the outer logarithmic layer. This interpolation formula was observed to reasonably align with the temperature profile behavior observed in experiments available at the time.

Pirozzoli (2023a) studied the statistics of passive scalars in pipe flow in the range of Prandtl numbers from $Pr = 0.00625$ to $Pr = 16$, using direct numerical simulation (DNS) of the Navier–Stokes equations, and introduced an eddy-viscosity model to obtain fully explicit predictions of the mean passive scalar profiles in the inner layer, and for the corresponding logarithmic offset function. Asymptotic scaling formulas were also derived for the thickness of the diffusive sub-layer, and for the heat transfer coefficient, which were found to accurately represent variations of both the Reynolds and the Prandtl number, for $Pr \gtrsim 0.00625$. A similar study of turbulent heat transfer in plane channel flows based on DNS data was carried out by Pirozzoli and Modesti (2023), who also reported predictive formulas for the heat transfer

* Corresponding author.
E-mail address: d.modesti@tudelft.nl (D. Modesti).

https://doi.org/10.1016/j.ijheatfluidflow.2024.109544
Received 19 February 2024; Received in revised form 16 June 2024; Accepted 14 August 2024
Available online 27 August 2024

coefficients under various thermal forcing conditions. In this paper, we use the pipe and channel flow DNS database to derive fully explicit analytical representations of the mean passive scalar profiles throughout the wall layer including the wake region, as a function of the Reynolds and Prandtl numbers, thus expanding on the work of Pirozzoli (2023a). This information is of outstanding practical importance as it can be used as a benchmark for low-order fidelity models like RANS, and it allows implementation of techniques of modal analysis (Taira et al., 2017). Although, as previously pointed out, the study of passive scalars is relevant in several contexts, one of the primary fields of application is heat transfer, and therefore from now on we will refer to the passive scalar field as the temperature field (denoted as T), and passive scalar fluxes will be interpreted as heat fluxes.

2. Predictive formulas

2.1. The inner layer

The starting point for the analysis of the mean temperature profile in the inner layer is the mean thermal balance equation, which in internal flows reads

$$\frac{1}{Pr}\frac{d\Theta^+}{dy^+} - \langle v\theta\rangle^+ = 1-\eta, \tag{1}$$

where $\theta = T - T_w$ expresses the temperature difference with respect to the wall, v is the wall-normal velocity, $\eta = y/\delta_t$, with y the wall distance, and δ_t a suitable measure of the thickness of the thermal layer, to be identified from case to case as later explained. Here and in the following, capital symbols are used to denote Reynolds averaged quantities, whereas lowercase symbols are used to denote fluctuations thereof, and angle brackets denote the averaging operator. In Eq. (1) the + superscript denotes normalization in wall units, whereby the friction velocity ($u_\tau = (\tau_w/\rho)^{1/2}$) is used for velocities, the viscous length scale ($\delta_v = \nu/u_\tau$) is used for lengths, and the friction temperature ($T_\tau = \alpha/u_\tau\,(d\langle T\rangle/dy)_w$) is used for temperature. The mean wall shear stress is τ_w, and ρ and ν and the fluid density and viscosity, respectively.

Modeling the turbulent heat flux $\langle v\theta\rangle$ in (1) requires closure with respect to the mean temperature gradient (see, e.g. Cebeci and Bradshaw, 1984), through the introduction of a thermal eddy diffusivity, defined as

$$\alpha_t = \frac{-\langle v\theta\rangle}{d\Theta/dy}. \tag{2}$$

Asymptotic consistency at the wall (Kader and Yaglom, 1972) requires that the turbulent flux scales as $-\langle v\theta\rangle^+ \sim y^3$, and Eq. (1) implies $\frac{d\Theta^+}{dy^+} \approx Pr + O(y^{+2}/\mathrm{Re}_\tau)$. Hence, the leading-order behavior of the thermal eddy diffusivity at the wall is

$$\alpha_t^+ = \frac{-\langle v\theta\rangle^+}{d\Theta^+/dy^+} \sim y^{+3}. \tag{3}$$

As noted by Pirozzoli (2023a), the thermal eddy diffusivity in the inner layer of wall-bounded flows has a relatively simple behavior, and it is very nearly universal with respect to variations of the Reynolds number. The thermal eddy diffusivity is also very much insensitive to variations of the Prandtl number, with exception of vanishingly small Prandtl numbers, in which limit α_t must vanish as conduction takes over. This is well portrayed in Figs. 1 and 4, which we will comment later on. The occurrence of a logarithmic layer in the mean temperature profile also implies $\alpha_t \sim y$ away from the wall, hence Pirozzoli (2023a) suggested the following functional expression to model the thermal eddy viscosity throughout the inner layer

$$\alpha_t^+ = \frac{(k_\theta y^+)^3}{(k_\theta y^+)^2 + C_\theta^2}. \tag{4}$$

Eq. (4) is inspired by the work of Musker (1979), who used a similar function to model the eddy viscosity in turbulent boundary layers. In Eq. (4) the thermal Kármán constant was determined to be $k_\theta \approx 0.459$ (Pirozzoli et al., 2022), and $C_\theta = 10.0$ was found based on scrutiny of DNS data for pipe flow. Whereas alternative functional expressions are possible, equation (4) bears the substantial advantage of being amenable to further analytical developments.

Starting from Eq. (1) and under the near-wall approximation ($\eta \ll 1$), one can infer the distribution of the mean temperature in the inner layer from knowledge of the eddy thermal diffusivity, by integrating

$$\frac{d\Theta^+}{dy^+} = \frac{Pr}{1+Pr\,\alpha_t^+}, \tag{5}$$

with α_t given in Eq. (4). The result of the integration yields the mean temperature profile in the inner layer

$$\begin{aligned}\Theta_i^+(y^+,Pr) = \frac{1}{2k_\theta\zeta_0(2+3Pr\zeta_0)}\Bigg\{&\frac{2\left(2\zeta_0+3Pr^2C_\theta^2\zeta_0+Pr(C_\theta^2+2\zeta_0^2)\right)}{\Delta}\\ &\times\left[\arctan\left(\frac{1+Pr\zeta_0}{\Delta}\right)-\arctan\left(\frac{1+Pr(2\zeta+\zeta_0)}{\Delta}\right)\right]\\ &+2Pr\left(C^2+\zeta_0^2\right)\log\left(1-\frac{\zeta}{\zeta_0}\right)\\ &+\left(Pr(2\zeta_0^2-C_\theta^2)+2\zeta_0\right)\log\frac{Pr\zeta^2+(1+Pr\zeta_0)(\zeta+\zeta_0)}{\zeta_0(1+Pr\zeta_0)}\Bigg\},\end{aligned} \tag{6}$$

where $\zeta = k_\theta y^+$, $\Delta = (3Pr^2\zeta_0^2 + 2Pr\zeta_0 - 1)^{1/2}$, and ζ_0 is the single (negative) real root of the cubic equation

$$Pr\zeta^3 + \zeta^2 + C_\theta^2 = 0, \tag{7}$$

whose exact solution is

$$\begin{aligned}\zeta_0 &= \frac{1}{3Pr}\left(-1+\frac{1}{z}+z\right),\\ z &= \left[\frac{1}{2}\left(-2-27Pr^2C_\theta^2+\sqrt{-4+\left(2+27Pr^2C_\theta^2\right)^2}\right)\right]^{1/3}.\end{aligned} \tag{8}$$

The temperature profiles given in Eq. (6) exhibit logarithmic behavior at $y^+ \gg 1$, namely

$$\Theta^+ = \frac{1}{k_\theta}\log y^+ + \beta(Pr), \tag{9}$$

where the log-law offset function is given by the following asymptotic expression (Pirozzoli, 2023a)

$$\begin{aligned}\beta(Pr) = \frac{1}{k_\theta}\Bigg[&\frac{2\pi C_\theta^{2/3}}{3\sqrt{3}}Pr^{2/3}+\frac{1}{3}\log Pr\\ &-\left(\frac{1}{6}+\frac{1}{2\sqrt{3}}+\frac{2}{3}\log C_\theta-\log k_\theta\right)\Bigg]+O(Pr^{-2/3}).\end{aligned} \tag{10}$$

Other synthetic profiles for the mean temperature in the inner layer are available in the literature. A notable example is the approach described by Cebeci and Bradshaw (1984), where the authors used the eddy-diffusivity and eddy-viscosity formulas from classical turbulence models to derive temperature profiles at arbitrary Prandtl numbers. Another example is the empirical correlations based on experimental-data fitting proposed by Kader (1981), which we use as reference in this study. The main advantage of the present framework compared to existing formulas is that Eq. (6) provides an explicit analytical expression for the mean temperature profiles based on a simple expression for the eddy diffusivity, which embeds the correct asymptotic behavior both close to the wall and in the logarithmic layer.

2.2. The core layer

The behavior of the mean temperature in the core (wake) region of wall-bounded flows was studied in terms of the temperature defect function by Pirozzoli et al. (2016) and Pirozzoli et al. (2021). The key finding was that the temperature defect profile (with respect to the peak value) is very nearly universal with respect to both Reynolds

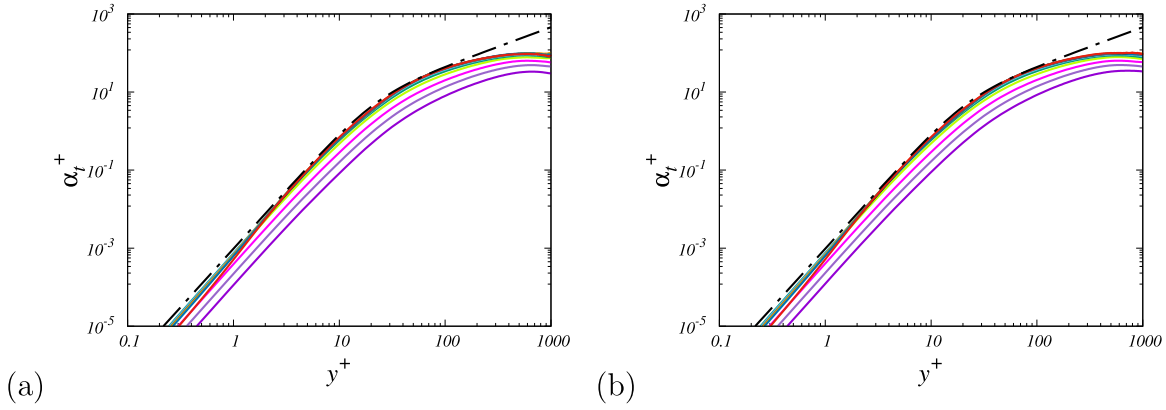

Fig. 1. Distributions of inferred eddy thermal diffusivity (α_t) as a function of wall distance for pipe flow with uniform internal heating (a) and constant heat flux (b), at various Pr, for $\mathrm{Re}_\tau = 1138$. The dash-dotted line denotes the fit given in Eq. (4). Color codes are as in Table 2. (For interpretation of the references to color in this figure legend, the reader is referred to the web version of this article.)

and Prandtl number variations, and the universal region encompasses a wide part of the flow thickness. Departures from outer-layer universality were only observed at $Pr \lesssim 0.025$, below which the similarity region becomes progressively confined to the outermost part of the thermal wall layer. As suggested by Pirozzoli et al. (2016, 2022), the core temperature profiles in internal flows can be closely approximated with simple universal quadratic distributions, which one can derive from (1) under the assumption of constant eddy thermal diffusivity. This assumption is analogous to the hypothesis of constant eddy viscosity proposed by Clauser (1956), also leading to a parabolic outer layer velocity distribution. A convenient analytical representation for the core mean temperature profile Θ_c is then

$$\Theta_e^+ - \Theta_c^+ = C_w (1-\eta)^2, \tag{11}$$

where Θ_e is the value of the mean temperature at the edge of the thermal wall layer.

2.3. Patching

An explicit approximation for the mean temperature profile throughout the thermal wall layer is then obtained by patching the inner-layer profile (6) with the core profile (11). Smooth patching is obtained by setting the transition point at the wall distance where the asymptotic logarithmic profile (9) and the core temperature profile (11) match and have equal first derivative. It is easy to show that continuity of the first derivatives is achieved provided the patching point is placed at the coordinate

$$\eta^* = \left(1 - \sqrt{1 - \frac{2}{C_w k_\theta}}\right) \Big/ 2, \tag{12}$$

whereas matching the values of the inner-layer and core temperature profiles implies that

$$\Theta_e^+ = \Theta_i^+(\eta^* \delta_t^+, Pr) + C_w \left(1-\eta^*\right)^2, \tag{13}$$

to be used in Eq. (11).

3. Results

3.1. Pipe flow

Results of DNS of thermal pipe flow are reported for the two canonical cases of uniform internal heating (UIH), and constant heat flux (CHF). In the former case the energy equation is forced with a spatially uniform internal heating term, in such a way that the bulk temperature is kept constant in time (Kim and Moin, 1989; Pirozzoli et al., 2016). In the latter case, the forcing term varies from point to point proportionally to u/u_b, such that the bulk temperature is also constant (Kawamura et al., 1999; Abe et al., 2004; Alcántara-Ávila et al., 2021). This second approach more precisely mimics the physical case of thermally developed flow in a duct with spatially and temporally uniform wall heating (Cebeci and Bradshaw, 1984). As discussed by Abe et al. (2004), Alcántara-Ávila et al. (2021), the thermal forcing strategy has small, but non-negligible effect on the temperature statistics. In both cases, the maximum temperature is attained at the pipe centerline, hence we assume the thermal wall layer thickness to be the pipe radius, and accordingly set $\delta_t = R$.

Table 1
Parameters for compound mean temperature profiles obtained by patching Eqs. (6) and (11). δ_t is the assumed thickness of the thermal layer, with R the pipe radius and h the channel half-thickness. C_θ is the inner-layer constant to be used in (4), C_w is the core profile constant to use in (11), and η^* is the outer-scaled coordinate of the patching point between the inner and the core temperature profiles.

Flow	Heating	δ_t	C_θ	C_w	η^*
Pipe	UIH	R	10.0	6.00	0.238
Pipe	CHF	R	10.0	7.00	0.193
Channel	UIH-sym	h	10.0	5.48	0.274
Channel	UIH-asym	$2h$	10.0	12.3	0.0982

A wide range of Reynolds and Prandtl numbers has been explored, spahnning Prandtl numbers from 0.0025 to 16 and friction Reynolds numbers $\mathrm{Re}_\tau (= Ru_\tau/\nu)$ ranging from 180 to 6000 (Pirozzoli et al., 2022; Pirozzoli, 2023b). A full scan of Prandtl numbers is here reported, for fixed bulk Reynolds number $\mathrm{Re}_b = 44\,000$, corresponding to friction Reynolds number $\mathrm{Re}_\tau \approx 1138$. The corresponding computational parameters are reported for reference in Table 2. In the table we also report some key global parameters as the friction Péclet number, $Pe_\tau = Pr\mathrm{Re}_\tau$, and the Nusselt number,

$$Nu = \mathrm{Re}_b\, Pr\, St, \tag{14}$$

with St the Stanton number, defined as

$$St = \frac{\alpha \left\langle \frac{dT}{dy} \right\rangle_w}{u_b \left(T_m - T_w\right)}, \tag{15}$$

where u_b is the bulk velocity and T_m is the mixed mean temperature (Kays et al., 1980). The table supports the generally accepted notion that the specific thermal forcing has little effect of the global thermal performance at Prandtl number of order unity or higher, however percent differences in the Nusselt number become significant at low Prandtl numbers.

The inferred eddy thermal diffusivities for all cases at $\mathrm{Re}_\tau = 1138$ are reported in Fig. 1. The agreement with the fit given in Eq. (4) is quite good in the inner layer, with deviations occurring only at $Pr \lesssim 0.025$.

Table 2
Flow parameters for DNS of pipe flow at various Prandtl number. N_z, N_r, N_ϕ denote the number of grid points in the axial, radial, and azimuthal directions, respectively; $Pe_\tau = Pr\,Re_\tau$ is the friction Péclet number; Nu is the Nusselt number (as defined in Eq. (14)), for cases with uniform internal heating (UIH), and constant heat flux (CHF). All DNS are carried out in a computational domain with length $L_z = 15R$, at bulk Reynolds number $Re_b = 44\,000$, corresponding to friction Reynolds number $Re_\tau \approx 1138$.

Pr	Mesh ($N_z \times N_r \times N_\phi$)	Pe_τ	Nu_{UIH}	Nu_{CHF}	Line style
0.00625	$1792 \times 164 \times 1793$	7.11	8.02	7.35	
0.0125	$1792 \times 164 \times 1793$	14.2	9.41	8.68	
0.025	$1792 \times 164 \times 1793$	28.5	12.6	11.6	
0.0625	$1792 \times 164 \times 1793$	71.1	21.5	20.2	
0.125	$1792 \times 164 \times 1793$	142.2	34.2	32.5	
0.25	$1792 \times 164 \times 1793$	284.4	53.8	51.4	
0.5	$1792 \times 164 \times 1793$	568.8	81.7	79.0	
1	$1792 \times 164 \times 1793$	1137.6	119.9	116.6	
2	$3584 \times 269 \times 3584$	2275.2	168.0	165.0	
4	$3584 \times 269 \times 3584$	4550.4	233.3	229.7	
16	$7168 \times 441 \times 7168$	18201.6	421.2	419.4	

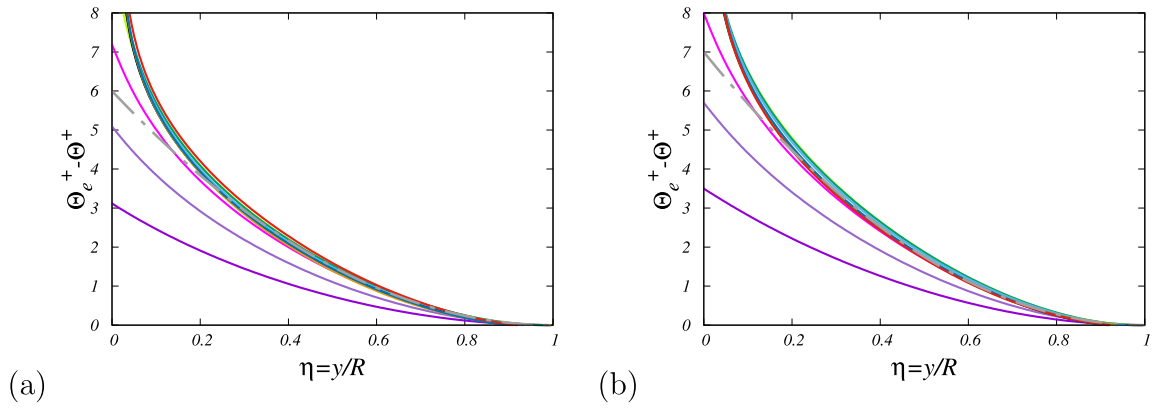

Fig. 2. Mean temperature defect profiles for pipe flow with uniform internal heating (a) and constant heat flux (b), at various Pr, for $\mathrm{Re}_\tau = 1138$. The dot-dashed line marks a parabolic fit of the DNS data ($\Theta^+ - \Theta^+_c = C_w(1-\eta)^2$), with values of C_w given in Table 1. Color codes are as in Table 2. (For interpretation of the references to color in this figure legend, the reader is referred to the web version of this article.)

Slight deviations from the DNS are found at $y^+ \lesssim 10$, where in any case the eddy diffusivity is much less than the molecular one. Notably, the influence of the thermal forcing (compare the two panels) seems to be entirely negligible. Universality with respect to Reynolds number variations has also been verified, but figures are omitted.

As for the temperature distribution in the core flow, in Fig. 2 we show the mean temperature profiles in defect form, referred to the pipe centerline properties. Again, the temperature profiles at fixed Re_τ are shown at various Prandtl numbers. As claimed in previous studies (Pirozzoli, 2023b), the figure supports close universality of the defect temperature profiles, for $\eta = y/R \gtrsim 0.2$. Furthermore, the figure confirms that the DNS data can be accurately fitted with the quadratic relationship (11). The fitting constant C_w, reported in Table 1 is a bit larger for the case of CHF forcing, on account of a stronger temperature defect. The universality of defect temperature profiles concerning variations in Reynolds number has been corroborated in prior literature (Pirozzoli et al., 2022), and is not reiterated here.

Based on the observed universality of the inner and outer layers with respect to Reynolds and Prandtl number variations, we proceed to apply the patching procedure outlined in Section 2.3, with fitting parameters listed in Table 1. The resulting temperature profiles are reported in Fig. 3, which confirms that the quality of the resulting patched temperature profiles is generally very good. Visible deviations are only evident at extremely low Prandtl numbers, as anticipated due to the absence of a genuine overlap layer. Discrepancies from the predicted trends are observed specifically at the lowest Prandtl numbers, which, as previously noted, deviate from the universal trend of α_t. In panel (b), we additionally present a comparison with the thermal law-of-the-wall proposed by Kays et al. (1980, Eqn.(14-4)) and the empirical correlation proposed by Kader (1981). To maintain clarity, only cases with $Pr \geq 1$ are depicted. The figure purports substantial overprediction of Θ^+ from the log-law formula of Kays et al. (1980). As for Kader's correlation, the general quality of the fit is more satisfactory, however an anomalous behavior is noticed in the buffer layer, and the shift in the log-law is somewhat overestimated at high Pr.

3.2. Channel flow

A similar analysis is herein reported for thermal channel flow, based on the DNS data of Pirozzoli and Modesti (2023). Two cases of thermal forcing are considered with uniform internal heating, whereby the two walls of the channel are either kept at the same temperature, hence heat is allowed to flow away through both walls, or one of the two walls is kept adiabatic. In the first case, referred to as symmetric heating (SYM), the maximum temperature is attained at the channel centerline, hence we assume the thermal wall layer thickness to be the channel half-thickness, $\delta_t = h$. In the second case, referred to as asymmetric heating (ASYM), the maximum temperature is attained at the adiabatic wall, hence we assume the thermal wall layer thickness to be the full channel thickness, $\delta_t = 2h$. Just as for pipe flow, a relatively wide range of Reynolds and Prandtl numbers has been explored, with $\mathrm{Re}_\tau (= hu_\tau/\nu)$ from 180 to 2000, and Pr from 0.025 to 4. A full scan of Prandtl numbers is here reported, for fixed bulk Reynolds number $\mathrm{Re}_b (= 2hu_b/\nu) = 40\,000$, corresponding to friction Reynolds number $\mathrm{Re}_\tau \approx 1002$. The key parameters for the DNS of channel flow are listed in Table 3.

Fig. 4 confirms that the inner-scaled thermal eddy diffusivity is universal across the range of Prandtl numbers under scrutiny, the only outlier being the case at the lowest Pr. In agreement with pipe flow, we find that Eq. (4) provides an excellent fit of the DNS data in the inner

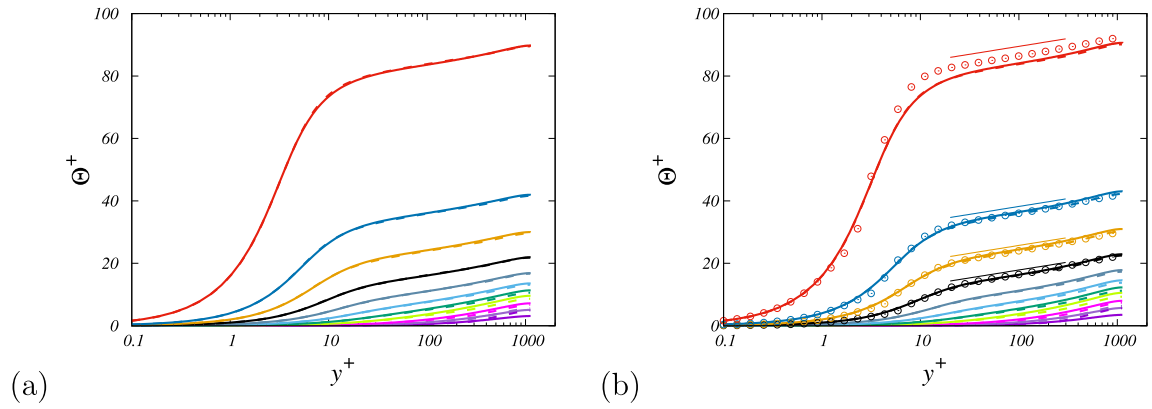

Fig. 3. Comparison of mean temperature profiles obtained from DNS (solid lines) with the prediction of the compound fitting function given by (6) and (11), with fitting parameters listed in Table 1 (dashed lines), for pipe flow with uniform internal heating (a) and with constant heat flux (b), at $\mathrm{Re}_\tau = 1138$. In panel (b) the circles denote the empirical predictions put forth by Kader (1981), and the thin lines the thermal law-of-the-wall of Kays et al. (1980). Color codes are as in Table 2. (For interpretation of the references to color in this figure legend, the reader is referred to the web version of this article.)

Table 3
Flow parameters for DNS of channel flow at various Prandtl number. N_x, N_y, N_z denote the number of grid points in the streamwise, wall-normal, and spanwise directions, respectively; $Pe_\tau = Pr\,Re_\tau$ is the friction Péclet number; Nu is the Nusselt number (as defined in Eq. (14)), for cases with symmetric heating (SYM), and asymmetric heating with one adiabatic wall (ASYM). All DNS are carried out in a computational domain with size $6\pi h \times 2h \times 2\pi h$, at bulk Reynolds number $Re_b = 40\,000$, corresponding to friction Reynolds number $Re_\tau \approx 1002$.

Pr	Mesh ($N_x \times N_y \times N_z$)	Pe_τ	Nu_{SYM}	Nu_{ASYM}	Line style
0.025	$1536 \times 298 \times 2304$	24.7	10.0	5.88	
0.25	$1536 \times 298 \times 2304$	247.3	44.6	32.7	
0.5	$1536 \times 298 \times 2304$	494.4	68.5	53.3	
1	$1536 \times 298 \times 2304$	1002.1	101.7	86.3	
2	$3072 \times 485 \times 4608$	2010.4	148.7	128.9	
4	$3072 \times 485 \times 4608$	4019.6	207.9	187.8	

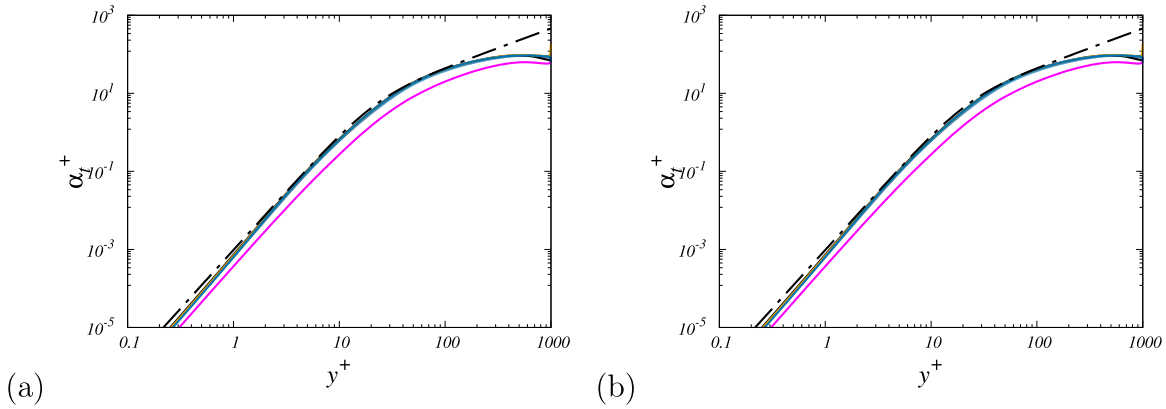

Fig. 4. Distributions of inferred eddy thermal diffusivity (α_t) as a function of wall distance, for plane channel flow with symmetric heating (a), and with asymmetric heating (b), at various Pr, for $\mathrm{Re}_\tau = 1002$. The dash-dotted line denotes the fit given in Eq. (4). Color codes are as in Table 3. (For interpretation of the references to color in this figure legend, the reader is referred to the web version of this article.)

layer, corroborating universality of the model for the temperature log-law shift function introduced by Pirozzoli (2023a), and whose validity was also proved for turbulent boundary layers (Balasubramanian et al., 2023).

The mean temperature defect profiles are shown in Fig. 5. In this respect, we note that the reference value is the mean temperature at the channel centerline in the case with symmetric heating (left panel), and the mean temperature at the adiabatic wall in the case of asymmetric heating (right panel). Just like the case of pipe flow, the simple quadratic fit (11), with suitably adjusted wake strength constants as given in Table 1 yields an excellent approximation for the temperature defect, the only outlier being the case at the lowest Pr. It is especially noteworthy that in the case of asymmetric heating the quadratic approximation fits accurately the DNS data in about 90% of the channel thickness.

Application of the patching procedure outlined in Section 2.3 yields the temperature profiles depicted in Fig. 6. In the case of symmetric heating (left), deviations from a logarithmic behavior are small, and the compound temperature law fits well the DNS up to the channel centerline. Deviations from the logarithmic behavior are on the other hand quite strong in the case of asymmetric heating. Again, the agreement with the DNS data is quite good, with observable deviations limited to the lowest Prandtl number case. The correlation provided by Kader (1981) also demonstrates reasonable performance in this scenario. However, it exhibits unnatural behavior in the buffer layer and tends to overpredict the strength of the wake.

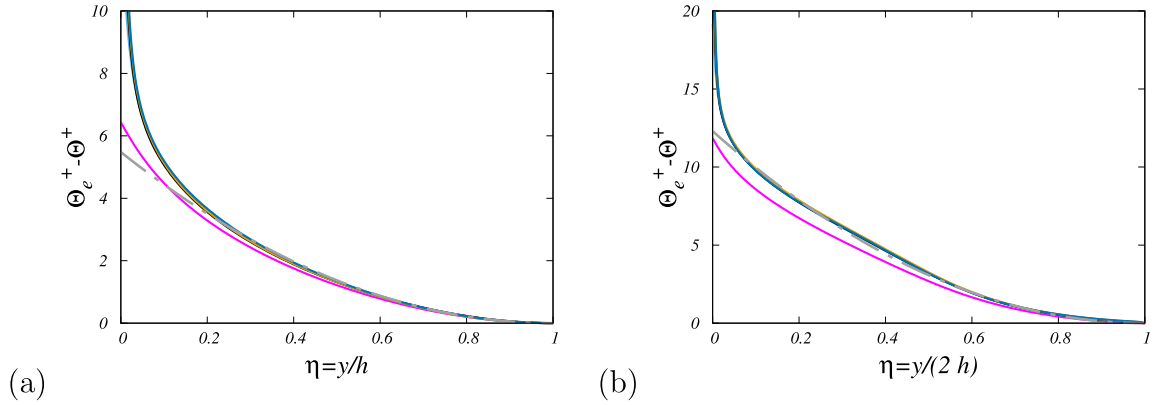

Fig. 5. Mean temperature defect profiles for channel flow with symmetric heating (a), and with asymmetric heating (b), at various Pr, for $\mathrm{Re}_\tau = 1002$. The dot-dashed line marks a parabolic fit of the DNS data ($\Theta_e^+ - \Theta_c^+ = C_w(1-\eta)^2$), with values of C_w given in Table 1. Color codes are as in Table 3. (For interpretation of the references to color in this figure legend, the reader is referred to the web version of this article.)

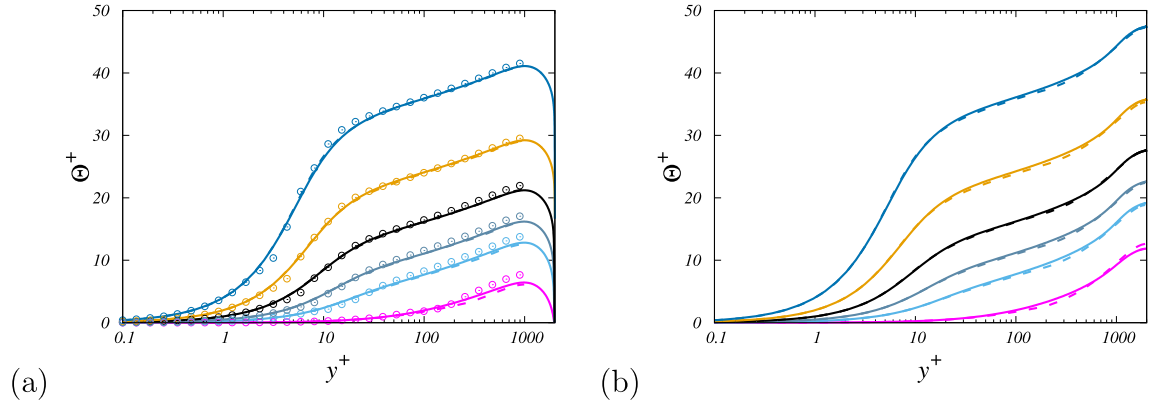

Fig. 6. Comparison of mean temperature profiles obtained from DNS (solid lines) with the prediction of the compound fitting function given by (6) and (11), with fitting parameters listed in Table 1 (dashed lines), for channel flow with symmetric heating (a) and with asymmetric heating (b), at $\mathrm{Re}_\tau = 1002$. The circles depicted in panel (a) represent the empirical predictions put forth by Kader (1981). Color codes are as in Table 3. (For interpretation of the references to color in this figure legend, the reader is referred to the web version of this article.)

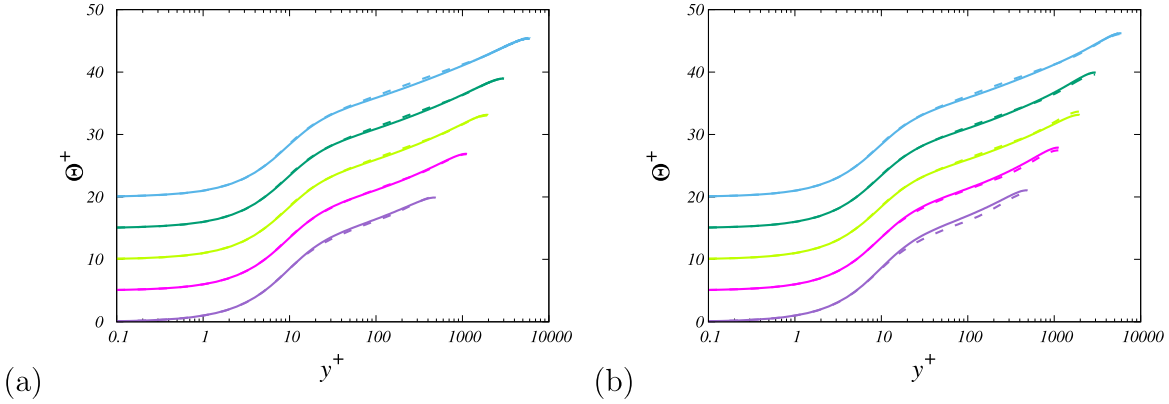

Fig. 7. Comparison of mean temperature profiles obtained from DNS (solid lines) with the prediction of the compound fitting function given by (6) and (11), with fitting parameters listed in Table 1 (dashed lines), for pipe flow with uniform internal heating (a) and with constant heat flux (b), at $Pr = 1$, for $\mathrm{Re}_\tau = 495, 1132, 1979, 3031, 6019$, from bottom to top, with offset of five wall units between consecutive values.

3.3. Reynolds number effects

Assessment of the Reynolds number dependence of our predictions is carried out in this section for the case of pipe flow, for which a wide range of Reynolds numbers has been explored (Pirozzoli et al., 2022), at unit value of the Prandtl number. The DNS data are compared with the analytical predictions herein developed in Fig. 7. Good agreement of the two distributions is generally found, which further supports universality of our predictions. However, some deviations are observed especially for cases with the lowest Reynolds number, and especially for the case of constant heat flux (panel (b)). This is not unexpected, as the logarithmic law of the wall for the mean temperature, which we leverage on, is known to apply only at sufficiently high Reynolds number that a sizeable overlap emerges between the inner and the outer part of the thermal layer. Further validation of our prediction would involve considering simultaneous Reynolds and Prandtl number variations. To date, no DNS database exists which densely covers the Re – Pr parameter space. However, having established universality of the inner layer with respect to Reynolds number variations, and universality of the outer layer with respect to Prandtl number variations, we see no reason why significant deviations from what herein observed for fixed value of the Reynolds number (Section 3.1) and for fixed value of the Prandtl number (present Section) should not apply to arbitrary combinations of the two parameters.

4. Conclusions

We have presented fully explicit approximations for the mean temperature (or concentration) profiles for forced convection in internal flows. The model relies on universality of the inner-scaled mean temperature profile in the inner wall layer with respect to Reynolds number variations, and universality of the mean defect temperature profile in the core layer with respect to both Reynolds and Prandtl variations. The explicit representation of the temperature profile (6) is used for the inner layer, which effectively incorporates effects from Prandtl number variation. A simple quadratic profile (11) is then used for the core temperature profile, which includes a single flow-adjustable constant, which accounts for geometric and/or thermal forcing effects of the temperature field away from the wall. A patching condition is derived which guarantees smooth transition between the inner and the core layer. Comparison with the DNS results shows excellent predictive capability of the model, in a wide range of Prandtl numbers, deviations becoming visible only at $Pr \lesssim 0.1$. As for the effects of Reynolds number variation, we find that the model predictions are accurate as long as a sensible logarithmic layer is present, which occurs when $Pe_\tau = Pr\,\mathrm{Re}_\tau \gtrsim 11$ (Pirozzoli, 2023b). We find that the present model constitutes a significant improvement over previous models developed for the prediction of the mean temperature distributions (Kader, 1981), as it yields much more realistic distributions within the wall layer as well as more accurate prediction of the shift of the log law with the Prandtl number. Given its modularity, the model lends itself to straightforward extension to cases with different flow geometry (e.g. boundary layers), and/or different heating conditions.

CRediT authorship contribution statement

Sergio Pirozzoli: Writing – review & editing, Writing – original draft, Software, Funding acquisition, Data curation, Conceptualization. **Davide Modesti:** Writing – review & editing, Conceptualization.

Declaration of competing interest

The authors declare that they have no known competing financial interests or personal relationships that could have appeared to influence the work reported in this paper.

Data availability

DNS data is available at http://newton.dma.uniroma1.it/ Synthetic temperature profiles and heat transfer coefficients can be generated using ThermoTurb web tool at http://www.thermoturb.com.

Acknowledgments

We acknowledge that the results reported in this paper have been achieved using the EuroHPC Research Infrastructure resource LEONARDO based at CINECA, Casalecchio di Reno, Italy, under a LEAP grant.

References

Abe, H., Antonia, R., 2009. Near-wall similarity between velocity and scalar fluctuations in a turbulent channel flow. Phys. Fluids 21, 025109.
Abe, H., Kawamura, H., Matsuo, Y., 2004. Surface heat-flux fluctuations in a turbulent channel flow up to $\mathrm{Re}_\tau = 1020$ with Pr= 0.025 and 0.71. Int. J. Heat Fluid Flow 25, 404–419.
Alcántara-Ávila, F., Hoyas, S., Pérez-Quiles, M., 2021. Direct numerical simulation of thermal channel flow for Re_τ= 5000 and Pr=0.71. J. Fluid Mech. 916, A29.
Antonia, R., Abe, H., Kawamura, H., 2009. Analogy between velocity and scalar fields in a turbulent channel flow. J. Fluid Mech. 628, 241–268.
Balasubramanian, A., Guastoni, L., Schlatter, P., Vinuesa, R., 2023. Direct numerical simulation of a zero-pressure-gradient turbulent boundary layer with passive scalars up to Prandtl number Pr=6. J. Fluid Mech. 974, A49.
Cebeci, T., Bradshaw, P., 1984. Physical and Computational Aspects of Convective Heat Transfer. Springer-Verlag, New York, NY.
Clauser, F., 1956. The turbulent boundary layer. Adv. Appl. Mech. 4, 1–51.
Dittus, F., Boelter, L., 1933. Heat transfer in automobile radiators of the tubular type. Int. Commun. Heat Mass Transfer 12, 3–22.
Gowen, R., Smith, J., 1967. The effect of the Prandtl number on temperature profiles for heat transfer in turbulent pipe flow. Chem. Eng. Sci. 22, 1701–1711.
Kader, B., 1981. Temperature and concentration profiles in fully turbulent boundary layers. Int. J. Heat Mass Transf. 24, 1541–1544.
Kader, B., Yaglom, A., 1972. Heat and mass transfer laws for fully turbulent wall flows. Int. J. Heat Mass Transf. 15, 2329–2351.
Kawamura, H., Abe, H., Matsuo, Y., 1999. DNS of turbulent heat transfer in channel flow with respect to Reynolds and Prandtl number effects. Int. J. Heat Fluid Flow 20, 196–207.
Kays, W., Crawford, M., Weigand, B., 1980. Convective Heat and Mass Transfer. McGraw-Hill.
Kim, J., Moin, P., 1989. Transport of passive scalars in a turbulent channel flow. In: André, J.-C., Cousteix, J., Durst, F., Launder, B.E., Schmidt, F.W., Whitelaw, J.H. (Eds.), Turbulent Shear Flows 6. Springer, pp. 85–96.
Kim, J., Moin, P., Moser, R., 1987. Turbulence statistics in fully developed channel flow at low Reynolds number. J. Fluid Mech. 177, 133–166.
Levich, V., 1962. Physicochemical Hydrodynamics. Prentice Hall, Englewood Cliffs. N.J.
Monin, A., Yaglom, A., 1971. Statistical Fluid Mechanics: Mechanics of Turbulence, vol. 1, MIT Press, Cambridge MA.
Musker, A., 1979. Explicit expression for the smooth wall velocity distribution in a turbulent boundary layer. AIAA J. 17, 655–657.
Nagano, Y., Tagawa, M., 1988. Statistical characteristics of wall turbulence with a passive scalar. J. Fluid Mech. 196, 157–185.
Pirozzoli, S., 2023a. An explicit representation for mean profiles and fluxes in forced passive scalar convection. J. Fluid Mech. 968, R1.
Pirozzoli, S., 2023b. Prandtl number effects on passive scalars in turbulent pipe flow. J. Fluid Mech. 965, A7.
Pirozzoli, S., Bernardini, M., Orlandi, P., 2016. Passive scalars in turbulent channel flow at high Reynolds number. J. Fluid Mech. 788, 614–639.
Pirozzoli, S., Modesti, D., 2023. Direct numerical simulation of one-sided forced thermal convection in plane channels. J. Fluid Mech. 957, A31.
Pirozzoli, S., Romero, J., Fatica, M., Verzicco, R., Orlandi, P., 2021. One-point statistics for turbulent pipe flow up to $\mathrm{Re}_\tau \approx 6000$. J. Fluid Mech. 926, A28.
Pirozzoli, S., Romero, J., Fatica, M., Verzicco, R., Orlandi, P., 2022. DNS of passive scalars in turbulent pipe flow. J. Fluid Mech. 940, A45.
Subramanian, C., Antonia, R., 1981. Effect of Reynolds number on a slightly heated turbulent boundary layer. Int. J. Heat Mass Transf. 24, 1833–1846.
Taira, K., Brunton, S., Dawson, S., Rowley, C., Colonius, T., McKeon, B., Schmidt, O., Gordeyev, S., Theofilis, V., Ukeiley, L., 2017. Modal analysis of fluid flows: An overview. AIAA J. 55, 4013–4041.